Spatial Extremes, Shapes of Large Waves, and Lagrangian Models

Hervé Socquet–Juglard and Kristian B. Dysthe, University of Bergen,
Karsten Trulsen, University of Oslo,
Sébastien Fouques, Jingdong Liu, and Harald E. Krogstad[1)], NTNU,
Trondheim

[1)] NTNU, Trondheim, Norway
harald.krogstad@math.ntnu.no

Abstract. The paper first states a simplified formulation of V. I. Piterbarg's theorem about extremes of Gaussian fields, which together with the Slepian Model Representation is a general tool for analyzing the spatial characteristics of ocean waves. We then consider numerical simulations of random surface gravity waves carried out in space and time by means of modified nonlinear Schrödinger equations. It is demonstrated that high waves in the simulations are steeper and more asymmetric than predicted by the Gaussian theory. The last part of the paper discusses Lagrangian stochastic models as alternatives to the conventional Eulerian first and second order models.

Introduction

Today we are starting to obtain spatial measurements of ocean waves by remote sensing techniques (Schulz-Stellenfleth and Lehner, 2004), and questions about spatial and even spatio/temporal extremes arise. For rogue waves the question naturally comes up whether such waves are truly exceptional, or whether they may actually happen somewhere or sometimes in a storm sea with considerable temporal and spatial extent.

Spatial data need tools from spatial statistics. The Slepian Model Representation (SMR) for Gaussian fields is well known [8]. In ocean engineering it forms the basis for *New Wave Theory* [17], the analysis of the shapes of extreme Gaussian waves [11], and the Boccotti theory of *Quasi Determinism* [1]. Another result of more recent origin is an explicit expression for the asymptotic extreme value distribution of a Gaussian field of arbitrary dimension derived by V. I. Piterbarg [14]. A simplified formulation of the theorem is given below.

The tools have been applied for analysis of spatial numerical simulations of random surface gravity waves of moderately narrow spectral bandwidth. The simulations utilize the Modified Nonlinear Schrödinger equations and produce the time development of sections of the ocean surface of the order 100×100 typical wavelengths and over 150 wave periods [18], [19]. Below we show a few results about the shape of the individual high waves. An extended discussion about extreme value distributions has been given elsewhere [16].

The final part reports from ongoing work investigating three dimensional second order Lagrangian stochastic models of the surface. Already at the first order, stochastic Lagrangian waves deviate significantly from linear Eulerian waves, and second order theory shows new and interesting features.

1 Gaussian Fields

Consider a zero mean homogeneous Gaussian field, $X(\mathbf{x})$, $\mathbf{x} \in \mathbb{R}^n$, with covariance function $\rho(\mathbf{x})$, $\rho(\mathbf{0}) = \sigma^2$, and spectrum $\Psi(\mathbf{k})$,

$$\rho(\mathbf{x}) = \int_{\mathbf{k}} e^{i\mathbf{k}\mathbf{x}} \Psi(\mathbf{k})\, d\mathbf{k}. \tag{1}$$

We shall assume that the covariance matrix, Λ, of $\nabla X = \{\partial X/\partial x_i\}_{i=1}^n$ is non-singular. The covariance matrix may be expressed as

$$\Lambda = \int_{\mathbf{k}} \mathbf{k}\mathbf{k}' \Psi(\mathbf{k})\, d\mathbf{k}. \tag{2}$$

By turning to the principal axis, Λ becomes diagonal and defines intrinsic spatial scales of the field, $\xi_k = 2\pi/\nu_k^{1/2}$, $k = 1, \cdots, N$, where ν_k is the k-th eigenvalue of Λ/σ^2. The scales define a *unit cell* with volume $|V| = \xi_1 \times \cdots \times \xi_n = (2\pi)^n \left|\Lambda/\sigma^2\right|^{-1/2}$. When $n = 1$ and $\mathbf{x}$ is time, the length of the unit cell is equal to the mean zero-upcrossing period, T_z. For $n = 2$ and $\mathbf{x} = (x_1, x_2)$, the scales are the mean wavelength, λ_0, and the mean crest length, λ_c, and $|V| = \lambda_0 \lambda_c$. For the space-time case, $(\mathbf{x}, t)$, an additional correction term due to the space-time correlation is needed, $|V| = \lambda_0 \lambda_c T_z \left(1 - C_{0t}^2 - C_{ct}^2\right)^{-1/2}$. Here C_{0t} is the correlation between $\partial X/\partial x_0(\mathbf{0}, 0)$ and $\partial X/\partial t(\mathbf{0}, 0)$, and similarly for C_{ct}.

The *Slepian Model Representation* (SMR) follows from the general theory of multivariate Gaussian variables, where conditional expectations and prediction errors are expressed in terms of the covariance functions. We shall only use the result for the behavior around a high maximum at $\mathbf{x} = \mathbf{0}$, where $\nabla X = 0$:

$$X_s(\mathbf{x}) = \{X(\mathbf{x}) \,|\, X(\mathbf{0}) = a, \nabla X(\mathbf{0}) = 0\} = a\frac{\rho(\mathbf{x})}{\rho(\mathbf{0})} + \Delta(\mathbf{x}). \tag{3}$$

The residual process $\Delta(\mathbf{x})$ is Gaussian with $\mathbb{E}(\Delta(\mathbf{x})) = 0$, and

$$\mathrm{Var}(\Delta(\mathbf{x})) = \rho(\mathbf{0}) - \frac{\rho(\mathbf{x})^2}{\rho(\mathbf{0})} - \nabla\rho(\mathbf{x})\, \Lambda^{-1} (\nabla\rho(\mathbf{x}))'. \tag{4}$$

The approximation $X_s(\mathbf{x}) \backsim a\frac{\rho(\mathbf{x})}{\rho(\mathbf{0})}$ is only reasonable when $\Delta(\mathbf{x})$ is small. In the present case this is at most for the extension of the unit cell centered at $\mathbf{x} = \mathbf{0}$, beyond which $\mathrm{Var}\,\Delta(\mathbf{x}) \to \sigma^2$.

Piterbarg's Theorem ([14], Theorem 14.1) considers homogeneous Gaussian fields in $\mathbb{R}^n$ and the asymptotic extreme value distributions for the maximum

of the field over subsets $T \subset \mathbb{R}^n$. We shall not bother about conditions on the shape of the subsets, and the rather strong regularity conditions on X required in the proof. Consider a subset T with volume $|T|$, or, recalling the unit cell V above, non-dimensional size $N = |T| / |V|$. Then the Piterbarg Theorem may be stated as

$$P\left(\max_{\mathbf{x}\in T} X(\mathbf{x}) \leq \sigma u\right) \backsim \exp\left[-(2\pi)^{\frac{n-1}{2}} e^{-u^2/2} H_{n-1}(u) N\right], \tag{5}$$

where H_n are Hermite polynomials w.r.t. to the standard Gaussian density ($H_0(u) = 1$, $H_1(u) = u$, $H_2(u) = u^2 - 1$, $\cdots$). Some care should be exercised with the expression in Eqn. 5, since it obviously fails for small values of u.

In one dimension, Eqn. 5 reduces to the expression following from Rice's Formula and the Poisson property of high up-crossings. This is an excellent approximation for the distribution of the maximum of Gaussian processes with ocean wave-like spectra. Being an asymptotic expression, it becomes more accurate as N increases, but the theorem gives no hint of how large N is needed. A limited simulation study with realistic ocean wave spectra has shown an excellent agreement for N as low as 20 for $n = 2$. In general, when N increases, the distributions tend asymptotically to a Gumbel distribution, $G(u) = \exp(-\exp(-a(u - u_0)))$, where

$$u_0 \approx x_0 + \frac{(n-1)\log(x_0)}{x_0},\ a = u_0 - \frac{(n-1)}{u_0},$$
$$x_0 = \sqrt{2\log N + (n-1)\log(2\pi)}. \tag{6}$$

As an illustration, consider a uniform "storm" over an area $100 \times 100\,\mathrm{km}$, lasting for 6 hours. With a mean zero-crossing wave period of 10 s, assume a mean wavelength to be 200 m, and a mean crest length of 750 m. Within the two-dimensional storm area there are at each instant of time about $N_2 = 6.6 \times 10^4$ "waves", and hence $u_0 = 5.23$. With the significant wave height $H_s = 4\sigma$, the most probable extreme crest height is

$$(\mathrm{Mode}\, C_{\max})_{space} = 1.31 H_s. \tag{7}$$

On the contrary, at a fixed location in space, $N_1 = 2160$, $u_0 = 3.94$, and

$$(\mathrm{Mode}\, C_{\max})_{time} = 0.99 H_s, \tag{8}$$

Finally the over-all highest crest, assuming a rough estimate of the space-time coherence so that

$$|V| \approx 6\lambda_0 \lambda_c T_z, \tag{9}$$

$N_3 = 2.4 \times 10^7$, and $u_0 = 6.73$. This results in

$$(\mathrm{Mode}\, C_{\max})_{space/time} = 1.68 H_s, \tag{10}$$

The last value is quite high, and it may indeed be pertinent to ask whether *freak waves* are real outliers from the standard statistics, or merely being at the wrong place at the wrong time. In addition, second wave theory will increase the numbers above even further.

Numerical Simulations

We refer to [3] for a discussion about the numerical simulation model based on the Modified Non-Linear Schrödinger(MNLS) equation. The numerical simulations shown below are all based on the evolution of a stochastic wave field with initial wave spectra based on the JONSWAP form and a cos-β directional distribution, $E(\omega,\theta) = S(\omega)\,D(\theta)$,

$$S(\omega) = \frac{\alpha}{\omega^5}\alpha \exp\left[-\frac{5}{4}\left(\frac{\omega}{\omega_p}\right)^4\right]\gamma^{\exp\left(-(\omega/\omega_p-1)^2/2\sigma_J^2\right)}, \tag{11}$$

$$D(\theta) = \begin{cases} \beta^{-1}\cos^2\left(\frac{\pi\theta}{2\beta}\right), |\theta| < \beta, \\ 0, \qquad\qquad \beta \le |\theta| \le \pi. \end{cases} \tag{12}$$

The corresponding wavenumber spectrum, truncated for $|\mathbf{k}-\mathbf{k}_0| > k_0$, is used for the initialization of the Fourier amplitudes. In all simulations, $k_p = 1$, and σ_J and γ have the standard average JONSWAP-values. The spectrum is scaled with α to an overall steepness $s = H_s/\lambda_p = 0.045$, typical for real ocean waves of some size. Only two different cases are shown below. For **Case A**, $\beta = 0.7$, corresponding to a directional spread $\sigma_1 = 14°$, and for **Case B**, $\beta = 0.35$, corresponding to $\sigma_1 = 7.2°$.

The simulated domain is square with sides $128\times\lambda_p$, and the simulations cover a time span of $150 \times (2\pi/\omega_p)$. During this time period the spectrum changes slowly, and this has some impact on the mean wave and crest lengths of the fields.

The SMR gives a stochastic description of the spatial shape of high maxima for Gaussian processes. The upper pair of plots in Fig. 1 shows a color-coded graph of the surface, reconstructed to 3rd order, around the maximum along with the SMR prediction for a Gaussian field with the same covariance function. We observe that the simulation shows a definitely narrower crest in the wave propagation direction, whereas the crest length is comparable to the SMR prediction. The SMR prediction drops to 0 quite fast away from the maximum and the prediction error, $\Delta(\mathbf{x})$, takes over. This is illustrated in the lower plots, where we show cuts through the maximum crest along the wave propagation direction and in the orthogonal direction to that, the wave crest direction. Plus/minus 2 standard deviations of $\Delta(\mathbf{x})$ are shown along with the actual outcome of the simulation on top, and we observe that the SMR prediction quickly becomes of limited value away from the peak.

In order to draw more firm conclusions about the shape of the surface around the crest, it is therefore necessary to average the simulations over several maxima and compare the mean to the SMR prediction. This is, however, somewhat tricky since the spectrum and hence the covariance function and the SMR vary over the time span of the simulations. An example using Case A, which undergoes only a minor spectral changes, is shown in Fig. 2. It is obvious that the average crest from the simulations is narrower than the SMR prediction, and the extension of the surrounding troughs is larger. When inspecting individual realizations, as

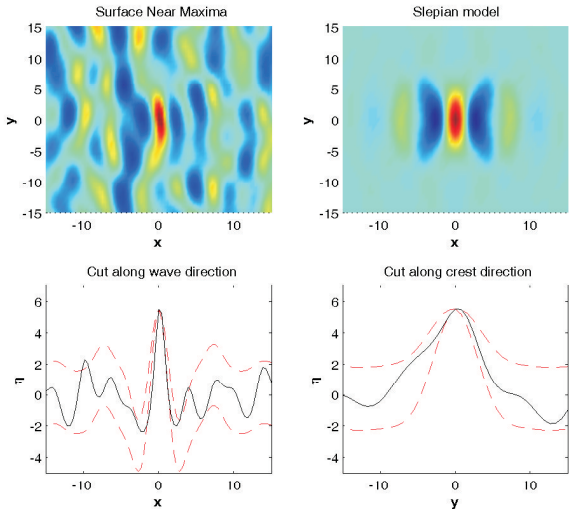

Fig. 1. Excerpt around the maximum peak of a simulation for Case A after $150T_p$. Top left: Color-coded surface elevation. Top right: SMR prediction. Bottom left: Cut through the maximum in the wave propagation direction. Black: Actual profile. Red: SMR prediction $\pm 2\,\mathrm{std}\,\Delta(\mathbf{x})$. Bottom right: Cut in the orthogonal (crest) direction.

shown in Fig. 1, it is often seen that the crests are longer than predicted by SMR, but bent in various directions. On the average, the crest length in the direction orthogonal to the main propagation direction is similar to the SMR. Figure 3 demonstrates this for cuts in the wave and orthogonal crest directions for both Case A and B. Along the wave propagation direction, the waves are steeper than predicted by the SMR. Moreover, as a consequence of the second order contribution, the troughs on each side are significantly shallower than linear wave theory predicts. The wave as a whole is therefore more vertically asymmetric. The average difference in crest lengths is minor, but this is an average in the orthogonal direction to the wave propagation, and not the length of the actual crests, which, as noted above, tend to be bent.

2 Lagrangian Models

The traditional ocean surface wave theory is based on a perturbation expansion of the Eulerian equations of motion for an incompressible and inviscid fluid. This approach has been applied successfully to model gross features of the waves as long as their overall steepness remains small. However, issues such as the estimation of radar backscatter from the sea surface depend strongly on the slope and curvature of the ocean surface on many scales. This requires a description of the waves which is rather difficult to achieve through the Eulerian approach.

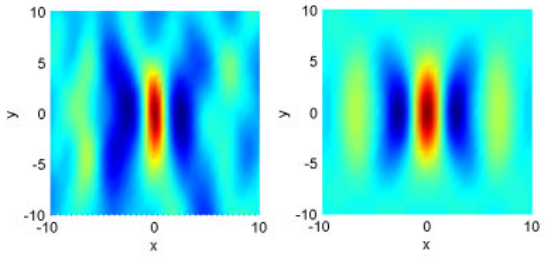

Fig. 2. Average surface shape around the maxima for Case A (left) compared to the SMR prediction, also averaged over the time span of the simulations (right).

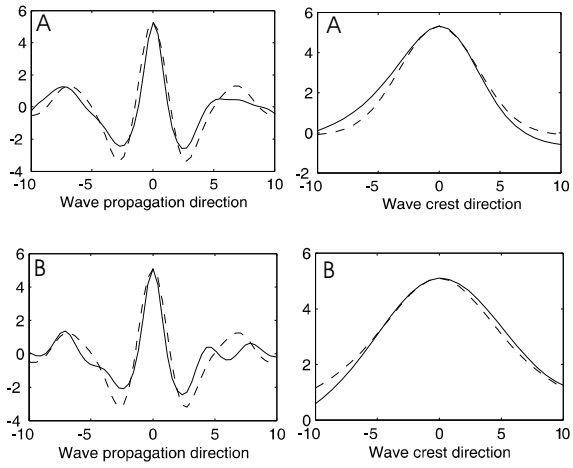

Fig. 3. Average cuts in the wave and crest directions for Case A (upper) and Case B (lower) . Solid: simulations, dashed: SMR prediction.

Recently, the interest for a Lagrangian description of ocean gravity waves has increased ([10], [2], [9], [5]). In this approach [6], one considers the motion of individual fluid particles, and the free surface is derived from the surface particles' positions [7]. As a result, the surface elevation is described through a parametric representation, which allows a larger flexibility as far as the wave shape is concerned.

In the Lagrangian model, the fluid is described through a set of fluid particles located at $\mathbf{X} = (x, y, z)^T$ at a given time t. The coordinate system has origin at the mean water level with z pointing upwards. Each particle is labelled by its reference position $\mathbf{X}_0 = (\alpha, \beta, \delta)^T$. The fluid is assumed to be incompressible and inviscid, and the flow irrotational. The conservation of momentum can then be integrated to

$$\nabla_L \times (\mathbf{J}\mathbf{X}_t) = \mathbf{0}, \tag{13}$$

and the mass conservation reads [7]

$$\det(\mathbf{J}) = 1, \tag{14}$$

where $\mathbf{J} \equiv \nabla_L^T \mathbf{X}^T$, $\nabla_L \equiv (\partial/\partial\alpha\, \partial/\partial\beta\, \partial/\partial\delta)$. The boundary conditions are

$$\begin{array}{l} \delta = 0 \quad \text{at the surface} \\ p = 0 \quad \text{for } \delta = 0 \\ z_t \to 0 \text{ for } \delta \to -\infty. \end{array} \tag{15}$$

A perturbation expansion of equations (13)–(15) has been carried out in [12] and [13]. According to dimensional analysis, the small parameter ϵ is proportional to $||\mathbf{J} - \mathbf{1}||$, where $\|\|$ is any matrix norm of $\mathbf{R}^{3\times3}$. Thus, ϵ is related to the Lagrangian gradient of the distance between the particles and their reference positions $\mathbf{X}_0$. This differs from the Eulerian approach, where the small parameter of the perturbation expansion is the wave slope. The displacement of the particles is now written as $\mathbf{X} = \mathbf{X}_0 + \mathbf{X}_1 + \mathbf{X}_2 + \cdots$, where $\mathbf{X}_n = O(\epsilon^n)$.

The first order solution is similar to the irregular extension of the Gerstner wave [4] given by Pierson (1961).

$$\mathbf{x}_1 = -\sum_p \frac{\mathbf{k_p}}{k_p} a_p e^{k_p \delta} \sin \Psi_p \tag{16}$$

$$z_1 = \sum_p a_p e^{k_p d} \cos \Psi_p \tag{17}$$

with $\Psi_p = \mathbf{k}_p \mathbf{x}_0 - \sigma_p t + \phi_p$, and where $k_p = |\mathbf{k}_p|$ and $\sigma_p^2 = g k_p$. The wave profiles show sharper crests and broader troughs. It is also capable of capturing some non-resonant wave-wave interactions such as the modulation of the crest-to-crest distance of short waves riding on the top of longer ones, as depicted in Fig. 4.

Besides, it can be shown that the interaction of two first order wave components with similar frequencies brings about a second order non-uniform current, whose main effect is to bend short crested waves. These so-called *horseshoe* patterns have also been observed to form in simulations based on the MNLS

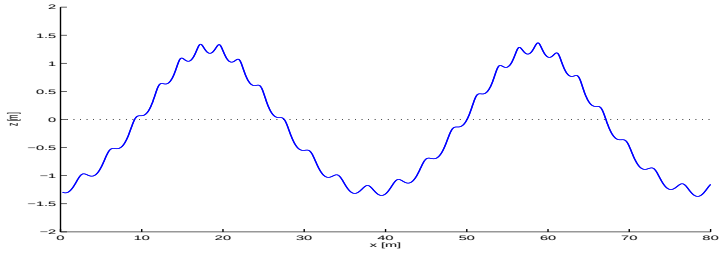

Fig. 4. First order bi-chromatic Lagrangian waves.

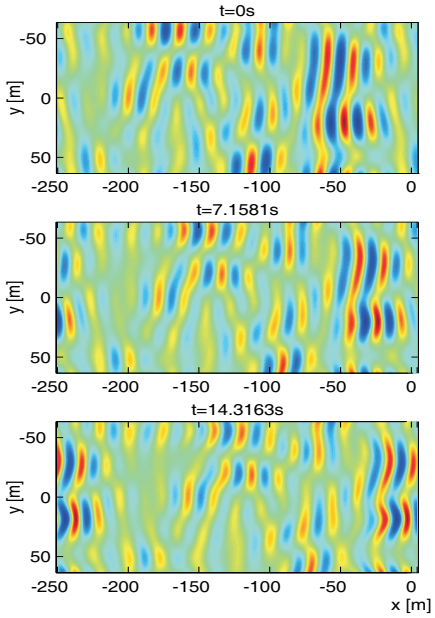

Fig. 5. Second order irregular Lagrangian waves in three dimensions developing "horse-shoe patterns".

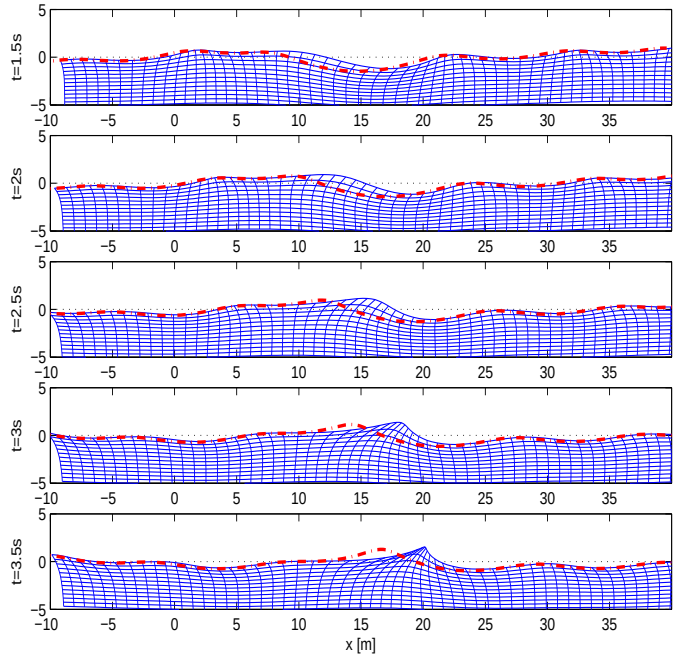

Fig. 6. Second order irregular Lagrangian waves (solid lines). Corresponding first order Lagrangian surface (dash-dotted line). The grid is regular in the reference coordinates.

equation [20], but are already seen at second order in the Lagrangian approach (see Fig. 5). The well-known Stokes drift is obtained from the second order interaction of a first order wave component with itself. Besides, for irregular waves, large horizontal displacement waves at the second order are responsible for asymmetric wave profiles with steep fronts, as shown in Fig. 6.

However, the second order mass transport induces an increase in the horizontal displacement of the fluid particles. Consequently, the small parameter of the perturbation expansion also grows towards infinity, and the duration of validity of the model is limited.

Conclusions

The Slepian Model Representation and Piterbarg's asymptotic extreme value distribution represent valuable tools for analyzing spatial fields. Piterbarg's Theorem gives a simple expression for the extreme values in Gaussian fields in any dimension, and may, in particular, answer questions about the maximum crest height in an area at a fixed time, or the overall highest crest in a spatially extended field lasting for some time.

The numerical simulations using the modified nonlinear Schrödinger equations give snapshots of the surfaces over a typical area 128×128 wavelengths and at time instances ranging from 0 to $150T_p$. During this time span, the simulated wave fields undergo some spectral change, as discussed in [3]. The simulated surfaces have been reconstructed to first, second and third order, and for the shape of the highest waves, the simulations show systematically steeper waves in the wave propagation direction and somewhat longer crests than the Gaussian prediction obtained from the SMR. Individual realizations often show that the crests bend. Simulated high waves are therefore significantly more vertically asymmetric than the corresponding Gaussian waves.

The Lagrangian stochastic models represent interesting alternatives to the conventional Eulerian models. Already at the first order, stochastic Lagrangian waves deviate significantly from linear Eulerian waves, and second order theory develops new and interesting features.

Acknowledgments

This research has been supported by the BeMatA programme of the Research Council of Norway (139177/431) and NTNU University Grant No. 70080000.

References

1. Boccotti, P. (2000), *Wave Mechanics for Ocean Engineering*, Elsevier, Amsterdam.
2. Chang, M.-S. (1969), Long-crested random graviy waves, *J. Geophys. Res.,* **74**(6), 1515–1536.
3. Dysthe, K. B., K. Trulsen, H. E. Krogstad, and H. Socquet-Juglard (2003), Evolution of a narrow band spectrum of random surface gravity waves, *J. Fluid Mech.,* **478**, 1–10.
4. Gerstner, F. J. (1809), Theorie der Wellen. *Gilbert's Annalen der Physik.*, xxxii.
5. Gjøsund, S. H. (2003), A Lagrangian model for irregular waves and wave kinematics. *Trans. of the ASME, Journal of Offshore Mechanics and Arctic Engineering,* **125**, 94–102.
6. Lagrange, J. L. (1788), *Mécanique Analytique*, Jacques Gabay, Paris. Reprint 1989.
7. Lamb, H. (1932), *Hydrodynamics*, Cambridge University Press, 6th edition.
8. Lindgren, G. (1972), Local maxima of Gaussian Fields, *Arkiv för Matematik*, **10**, 195–218.
9. Moe, G., Ø. A. Arntsen, and S. H. Gjøsund (1998), Wave kinematics based on a Lagrangian formulation. *Proc. of the 1998 International OTRC Symposium "Ocean Wave Kinematics, Dynamics and Loads on Structures"*, ASCE Press, 56–63.
10. Phole, F. V. (1950), *The Lagrangian equations of hydrodynamics: solutions which are analytic functions of the time*,0 Ph.D. Thesis, Graduate School of Arts and Science, New York University.
11. Phillips, O. M., D. Gu, and E. J. Walch (1993), On the Expected Structure of Extreme Waves in a Gaussian Sea. Part II: SWADE Scanning Radar Altimeter Measurements, *J. Phys. Ocean.*, **23**, 2297–2309.
12. Pierson, W. J. (1961), Models of random seas based on the Lagrangian equations of motion, *Tech. Rept. Contr. Nonr-285(03).* College of Engineering, Research Division, New York University.

13. Pierson, W. J. (1962), Perturbation analysis of the Navier-Stokes equations in the Lagrangian form with selected linear solutions, *J. Geophys. Res.,* **67**(8), 3151–3160.
14. Piterbarg, V. I. (1996), *Asymptotic Methods in the Theory of Gaussian Processes and Fields*, AMS Transl. of Math. Monographs, **148**, Providence, R.I.
15. Schulz-Stellenfleth, J. and S. Lehner (2004), Measurement of two dimensional sea surface elevation fields from complex synthetic aperture radar data, *IEEE Trans. Geos. Rem. Sensing*, **42**(6), 1149 – 1160.
16. Socquet-Juglard, H., K. B. Dysthe, K. Trulsen, H. E. Krogstad, and J. Liu (2004), Probability distributions of surface gravity waves during spectral changes, submitted to *J. Fluid Mech.*
17. Tromans, P. S., A. R. Anatürk, and P.M. Hagemeijer (1991), A new model for the kinematics of large ocean waves – applications as a design wave, in Proc. 1st Int. Offshore and Polar Engng. Conf., Edinburgh, UK, **3**, 54–71.
18. Trulsen, K. and K. B. Dysthe (1996), A modified nonlinear Schrödinger equation for broader bandwidth gravity waves on deep water, *Wave Motion,* **24**, 281–289.
19. Trulsen, K., I. Kliakhandler, K. B. Dysthe, and M. G. Velarde (2000), On weakly nonlinear modulation of waves on deep water, *Phys. Fluids,* **2**, pp. 2432–2437.
20. Trulsen, K. (2004), Large horseshoe patterns of water surface waves, submitted *J. Fluid Mech.*